The Application of Iterated Defect Corrections Based on WENO Reconstruction

Alexander Filimon and Claus-Dieter Munz

Abstract. In this article we apply the procedure of the iterated defect correction method to the Euler equations as well as to the Navier-Stokes equations. One building block in the defect correction approach is the lower order basic method, usually first or second order accurate. This scheme gives a steady solution of low accuracy as the starting point. The second building block is the WENO reconstruction step to estimate the local defect. The local defect is put into the original equation as source on the right hand side with a minus sign. The resulting modified equation is then again solved with the low order scheme. Due to the source term with the local defect the order of accuracy is iteratively shifted to the order of the reconstruction. We show numerical results for several validation test cases and applications.

1 Introduction

Numerical simulations of the equations of fluid mechanics contain unavoidable errors due to several necessary approximations. To analyze these errors is crucial for the evaluation of the reliability of the numerical results. In the following we focus ourselves to the discretization errors. This means, that the modeling errors are excluded and the exact solution of the governing equations is supposed to be the reference solution of the described physical phenomenon.

The discretization errors can be separated into local and global discretization errors. By inserting the exact solution into the discretized equations, the local discretization error, also known as the local defect of a numerical approximation, can be determined. The more significant global discretization error gives the difference

Alexander Filimon · Claus-Dieter Munz
Institute of Aerodynamics and Gas Dynamics, 70569 Stuttgart, Germany
e-mail: {filimon,munz}@iag.uni-stuttgart.de

B. Eisfeld et al. (Eds.): *Management & Minimisation of Uncert. & Errors*, NNFM 122, pp. 129–154.
DOI: 10.1007/978-3-642-36185-2_6

between the numerical and the exact solution. In both cases the exact solution is needed, which makes the error approximation for real applications cumbersome. A common approach is to run the same problem on several meshes with different step size h. A mesh convergence study allow then to compute the so called experimental convergence rate. Finally, a Richardson extrapolation can be used to determine the best approximate solution together with an estimation of the global discretization error. In practical 3D applications with complex geometries, this approach becomes cumbersome and sometimes even unfeasible because of the high computational costs. Our approach allows an error approximation for steady problems on the original mesh by using a polynomial reconstruction within the defect correction method.

Starting with a steady solution of a first or second order accurate finite volume scheme, we employ the modified weighted essentially non oscillatory (WENO) reconstruction scheme of Dumbser and Käser [4] for unstructured meshes. The resulting polynomial distribution allows an improved flux computation which can be applied to estimate the local discretization error. The method of the iterated defect correction (IDeC) consists of subtracting this local defect as a source term on the right hand side of the original equations [23, 19]. The now modified equations are solved with the original method of first or second order accuracy, in the following also called the basic method or the basic scheme, resulting into a new corrected steady solution. A further reconstruction of the corrected solution yields a better estimation of the local defect which is now used in the modified equations. Iteratively applied, the method of the defect correction shifts the order of accuracy of the basic scheme to the higher order of the used reconstruction. By this approach, an approximation of the global discretization error up to an accuracy of the higher order reconstruction is available.

2 The Method of Iterated Defect Correction

The defect correction approach was originally proposed by Zadunaisky ([22], [23]) for the estimation of the global discretization error in ordinary differential equations. The method was then generalized by Stetter [18] who introduced the iterative procedure which is applied in this work to partial differential equations. A number of theoretical investigations were done for ordinary differential equations by Frank ([5], [6]). Further papers of Pereyra ([15], [14]) show a different way of applying the defect correction method and gives additional analysis of the method. A nice overview on the defect correction approach can be found in Stetter [19] where he gives an overview of the different procedures. The proposed iterative defect correction method in this work is based on the procedure introduced by Stetter in [18] for ordinary differential equations. As was shown by Frank and Ueberhuber in [7] the iterated defect correction can also be applied on partial differential equations.

For the sake of simplicity we describe in the following the employed iterated defect correction on the example of a scalar one dimensional evolution equation

$$u_t + f(u)_x = 0, \tag{1}$$

keeping in mind that the whole procedure can be extended to multi dimensions and to diffusion fluxes which additionally depend on ∇u, as it is the case for the Navier-Stokes equations. As mentioned before, we focus on steady solutions, i.e., $u_t = 0$. The time dependence in (1) is used only for the iteration of the approximate solution to a steady state. Conform with the convention in the cited papers we write the equation (1) in the abstract form

$$L_h u_h = r_h \qquad \text{with} \qquad Lu \equiv \frac{\partial f}{\partial x}, \tag{2}$$

where the operator L is the exact linear or nonlinear differential operator and L_h is the discretized operator with the mesh width parameter h. For L_h we impose a stable, consistent and fast invertible operator, which is easily achieved by an operator with a low consistency order of one or two. For the theory of the iterated defect correction the operator L_h can also be of higher order. For practical calculations it is more interesting to correct a first or second order accurate method which is often applied in practice. Equation (2) will be called the basis method with the solution u_h computed by inversion of the operator L_h:

$$u_h = L_h^{-1} r_h. \tag{3}$$

Additionally we need another numerical method for the original problem (1) on the same mesh, but with a higher consistency order

$$S_h w_h = r_h. \tag{4}$$

(4). This higher order discretization will only be used to estimate the local defect and is applied once per defect iteration in that form. Instead of solving directly the higher order discrete problem which may need a lot of time and development of the solution procedure, the modified problem

$$L_h u_h = r_h - d_h \tag{5}$$

is solved using the basic method (2). With $d_h = S_h w_h - L_h u_h$ the local defect we apply equation (5) iteratively

$$L_h u_h^{[k+1]} = r_h - d_h^{[k+1]} \qquad k = 1, 2, 3, \ldots, N_{IDeC} \tag{6}$$

with the defect iteration index k and N_{IDeC} the maximum defect correction iterations, converging towards the solution w_h, the reconstruction polyomial higher order. The whole defect correction procedure can be formulated in the following step by step description.

1. We start with a steady solution

$$u_h^{[0]} = L_h^{-1} r_h^{[0]} \qquad \text{with} \qquad r_h^{[0]} = r_h \tag{7}$$

of our basic method (2). The approximated solution u_h is then reconstructed with the weighted essentially non oscillatory scheme, which will be described in section 3. The reconstruction produces a polynomial distribution $w_h^{[k]}$ of the integral average in each grid cell.

2. Applying now the operator of higher order consistency S_h to the reconstructed solution $w_h^{[k]}$ we compute the local defect $d_h^{[k+1]}$ for the next defect correction iteration $k+1$:

$$\begin{aligned} d_h^{[k+1]} = S_h w_h^{[k]} - r_h^{[k]} &= S_h w_h^{[k]} - L_h u_h^{[k]}, \\ r_h^{[k]} &= r_h - d_h^{[k]}. \end{aligned} \tag{8}$$

3. This defect is then subtracted as a source term on the right hand side of equation (2) and the modified equation

$$\begin{aligned} L_h u_h^{[k+1]} &= r_h - d_h^{[k+1]} \\ &= r_h - \left(S_h w_h^{[k]} - L_h u_h^{[k]} \right) \end{aligned} \tag{9}$$

is solved with the basic method, applying the inverse operator L_h^{-1}. One gets then the corrected solution $u_h^{[k+1]}$ after the k-th defect iteration, converging for

$$L_h u_h^{[k+1]} \approx L_h u_h^{[k]}. \tag{10}$$

With this convergence criteria, equation (9) reduces to the method higher order (4), with w_h the reconstruction polynomial.

Equation (5) is also called the "neighboring problem" with respect to the original formulation of the defect correction by Zadunaisky. For the process of iterated defect correction one must assume that (6) and (2) are neighboring mathematical problems. Since w_h represents a polynomial reconstruction of the basic solution u_h on the same mesh, the defect d_h as defined in equation (8) is "small" and so the assumption of the "neighboring problem" is plausible.

As we use a finite volume scheme for the basic method we can write the modified equation (5) in a semi discrete form defined on the interval $[x_{i-\frac{1}{2}}, x_{i+\frac{1}{2}}] \mathrm{x} [t^n, t^n + \Delta t]$ with $u_i = u_h$, being the discrete state in the cell i, as

$$\Delta u_i^{[k+1]} = -\frac{1}{\Delta x} R(u_i^{[k+1]}) - \frac{1}{\Delta x} \underbrace{\left(R(w_i^{[k]}) - R(u_i^{[k]}) \right)}_{d_h^{[k+1]}} \tag{11}$$

with

$$R(\mathscr{Q}_i) = \int_{t^n}^{t^n+\Delta t} \int_{x_{i-1/2}}^{x_{i+1/2}} f(\mathscr{Q}_i)_x dx dt, \tag{12}$$

whereas $\mathscr{Q}_i$ is considered as a placeholder for $u_i^{[k]}, u_i^{[k+1]}$ and $w_i^{[k]}$. As common for a finite volume approach the unknown physical flux $f(\mathscr{Q}_i)$ is replaced by an appropriate numerical flux approximation $g_{i+\frac{1}{2}}$ on the cell border of two adjacent cells. The numerical flux depends only on the states left and right of the cell interface: $g_{i+\frac{1}{2}} = g(\mathscr{Q}^-_{i+\frac{1}{2}}, \mathscr{Q}^+_{i+\frac{1}{2}})$, with $\mathscr{Q}^-$ defining the state on the interface in the cell itself and $\mathscr{Q}^+$ being the state on the interface in the neighboring cell. If we choose as a simple example a basic method of first order in time and space, equation (11) yields

$$\Delta u_i^{[k+1]} = -\frac{\Delta t}{\Delta x}\left(g(u_{i+\frac{1}{2}}^{[k+1],-}, u_{i+\frac{1}{2}}^{[k+1],+}) - g(u_{i-\frac{1}{2}}^{[k+1],-}, u_{i-\frac{1}{2}}^{[k+1],+})\right) - d_h^{[k+1]} \tag{13}$$

with

$$\begin{aligned} d_h^{[k+1]} = {} & \frac{\Delta t}{\Delta x}\left(g(w_{i+\frac{1}{2}}^{[k],-}, w_{i+\frac{1}{2}}^{[k],+}) - g(w_{i-\frac{1}{2}}^{[k],-}, w_{i-\frac{1}{2}}^{[k],+})\right) \\ & - \frac{\Delta t}{\Delta x}\left(g(u_{i+\frac{1}{2}}^{[k],-}, u_{i+\frac{1}{2}}^{[k],+}) - g(u_{i-\frac{1}{2}}^{[k],-}, u_{i-\frac{1}{2}}^{[k],+})\right) \end{aligned} \tag{14}$$

an approximation of the corrected state $u_h^{[k+1]}$ in the cell i. We point out that the integral of the higher order fluxes $f(w_h^{[k]})$ have to be computed with an appropriate numerical integration of accuracy higher than the one of the basic method. In the case of 1D there is no need of such an integration, the interface being the only integration point. For 2D or 3D discretizations an efficient integration scheme is necessary. In our case we use Gauss quadrature. This leads to an approximation of the flux integral in cell i as

$$\int_{\partial C_i} g\left(w_i^{[k],-}, w_i^{[k],+}\right)\mathbf{n} dS \approx \sum_{K\in\partial C_i}\sum_{j=1}^{n_{GP}} \omega_j^K g\left(w_{i,j}^{[k],+}, w_{i,j}^{[k],-}\right)\mathbf{n}_K S_K, \tag{15}$$

where n_{GP} and ω_j^K denote the number and the weights of the Gauss integration points j on the interface K, respectively, S_K is the length or the surface and $\mathbf{n}_K$ is the outward pointing unit normal vector. If the polynomial degree of the reconstruction is chosen to be $p' > p$, with p, being the polynomial degree of the basic method, we take $n_{GP} = \frac{p'+1}{2}$ for the 2D case, which is accurate up to a polynomial degree of p'. In the 3D case we use a rather sub-optimal number $n_{GP} = (\frac{p'+1}{2})^2$ of Gauss points which is nevertheless accurate up to a polynomial degree p'.

2.1 IDeC for Inhomogeneous Problems

For inhomogeneous equations the method of iterated defect correction can be applied in two different ways, which leads both to the same corrected solution but with different time efficiencies. The difference is even bigger for source terms depending on the solution itself. In the following work we will present both inhomogeneous equations with source terms depending only on space and source terms including the solution itself. To describe the different formulations we take the scalar evolution equation

$$u_t + f(u)_x = s(u). \tag{16}$$

again in 1D as example with the source term s depending on the solution u. If we apply the iterated defect correction on this problem as done before, computing the local defect only in the flux terms, we can write the modified equation (5) as

$$u_t^{[k+1]} + f(u^{[k+1]})_x = s(w) - \underbrace{\left(f(w^{[k]})_x - f(u^{[k]})_x\right)}_{d^{[k+1]}}. \tag{17}$$

The integration of each term is done as shown above what leads to a similar semi discrete representation of the modified equation (5) with the additional integral

$$\int_{t^n}^{t^n+\Delta t} \int_{x_{i-1/2}}^{x_{i+1/2}} s(w_i) dx dt,$$

of the source term s in the cell i. To achieve the consistency order of the reconstruction in the iterated defect correction procedure with the above formulation (17), it is important to compute the source term with the high order accuracy. This implies a reconstruction in each iteration of the basic method and in 2D and 3D an integration with much more Gauss points than used for the basic scheme of lower order is necessary. The high computational cost can be reduced by reformulating the problem in equation (17). Instead of taking only the fluxes into account for the local defect, we propose to include the source term as well in the definition of the local defect. This yields

$$u_t^{[k+1]} + f(u^{[k+1]})_x = s(u^{[k+1]}) - \underbrace{\left[f(w^{[k]})_x - s(w^{[k]}) - \left(f(u_h^{[k]})_x - s(u^{[k]})\right)\right]}_{d^{[k+1]}}, \tag{18}$$

a new modified equation where the source term in the iteration of the basic scheme is now integrated with the lower order accuracy whereas the reconstruction of the source term is only done once per defect iteration to compute the local defect.

3 WENO Reconstruction on Unstructured Grids

In order to compute the higher order operator for the grid cell $C_{(i)}$ a reconstruction of the cell averages defined

$$\bar{u}_{(i)} = \frac{1}{\left|C_{(i)}\right|} \int_{C_{(i)}} u dV \tag{19}$$

is done, where $\left|C_{(i)}\right|$ is the length, the surface or the volume of the gird cell depending on the space dimension. To ensure a stable reconstruction even at discontinuities, a high order Weighted Essentially Non Oscillatory (WENO) reconstruction was chosen. This method was first introduced by Shu et al. [11, 10] and Osher et al. [13]. For the proposed defect correction method, the modified reconstruction algorithm by Dumbser et al. [4] is used which ensures a robust method on 2D and 3D unstructured meshes even with distorted cells [4] eliminating scaling and bad conditioning problems common to WENO reconstruction technique.

In this approach, the reconstructed polynomial is built by a linear combination of orthogonal basis functions as given in [3] for triangles in 2D and tetrahedrons in 3D. We write the reconstruction polynomial for the element $C_{(i)}$ as

$$w_{(i)}(\xi,\eta,\zeta) = \sum_{l=1}^{L} \hat{w}_{(i)_l} \Psi_l(\xi,\eta,\zeta), \tag{20}$$

with ξ,η and ζ the coordinates in the reference coordinate system. Unlike the common WENO reconstructions at discrete cell points, the basis polynomials are continuously extended over the whole stencil and are then restricted to the considered element $C_{(i)}$ after having obtained a reconstruction polynomial. The number of degrees of freedom L being $L = \frac{1}{2}(M+1)(M+2)$ in 2D and $L = \frac{1}{6}(M+1)(M+2)(M+3)$ in 3D depends on the polynomial degree M of the basis functions Ψ_l. Whereas the basis functions are space dependent, the reconstructed degrees of freedom $\hat{w}_{(i)_l}$ depend only on time.

Similar to the finite element framework, the reference space is the unit element C_U. This is a triangle with the canonical coordinates $(0,0),(0,1)$ and $(1,0)$ in 2D and a tetrahedron with the canonical coordinates $(0,0,0),(0,0,1),(0,1,0)$ and $(1,0,0)$ in 3D. The transformation from the physical space $x-y-z$ into the reference space $\xi-\eta-\zeta$ can be done by a linear transformation matrix (see [4]). To perform the reconstruction, several stencils have to be chosen which is done in the reference space. There are three groups which are defined as follows:

1. First the central stencil is built by adding successively Neumann neighbors, i.e. immediate side neighbors of the considered cell $C_{(i)}$, to the stencil until the desired number of cells n_e in one stencil is reached. The size of n_e will be discussed later on in this chapter.

2. The following stencils, three of them in 2D and four in 3D, are chosen out of the primary sectors. As mentioned before this is done in the reference space ξ, η, ζ. So the primary sectors are spanned by the vectors starting from each vertex of the unit element C_U along the edges intersecting this vertex. Transformed elements are then successively added to the stencils.
3. As shown by Käser and Iske [12] it is favorable to take one more family of stencils into account than the two mentioned above. Although this increases the computational effort it ensures a stable and robust reconstruction in 2D and 3D configurations for special locations of the discontinuities. Additionally it improves the one sided reconstruction, e.g. at walls. The so-called reverse sectors are spanned by the negative vectors of each primary sector defined above.

This sums up to $n_s = 7$ and $n_s = 9$ stencils in 2D and 3D which are used for the reconstruction. At the domain boundaries or for the case that not all stencils could be filled up due to geometrical reasons, the total number of stencils n_s can decrease.

For a conservative reconstruction one must assure that the polynomial distribution w_i in each cell $C_{(i)}$ of the stencil m conserves the integral mean value of the cell at hand $C_{(i_s)}$.

$$\frac{1}{\left|C_{(i_s)}\right|} \int_{C_{(i_s)}} w_{(i)}(\xi) dV = \bar{u}_{(i_s)} \tag{21}$$

The evaluation of the conservation condition is carried out in the reference space. This is done by applying linear transformation matrix with respect to the element $C^{(i)}$ to each cell in the stencil, where the transformed elements are in the following denoted by $\tilde{C}_{(i)}$. Taking into account that the degrees of freedom $\hat{w}_{(i)}$ are not space dependent, the above equation results in

$$|J| \sum_{l=1}^{L} \left(\int_{\tilde{C}_{(i_s)}} \Psi_l(\xi) d\xi d\eta d\zeta \right) \hat{w}_{(i)_l} = |J| \left|C_{(i_s)}\right| \bar{u}_{(i_s)}. \tag{22}$$

The Jacobian determinant which is introduced due to the transformation appears on both sides of equation (22), so it cancels out and with it scaling effects are eliminated as well. Furthermore, Abgrall reports in [1] that ill-conditioned reconstruction matrices are also avoided through this effect.

As the transformation to canonical coordinates is only done for the reconstructed cell, the integration in equation (22) turns out to be non-trivial. This is not the case if a second transformation with respect to the reconstructed cell is done additionally. For more details see [4]. With it, the left hand side of equation (22) can again be easily integrated using the Gaussian quadrature with an appropriate accuracy. This yields the following linear system which have to be solved for the reconstructed degrees of freedom.

$$\underline{\underline{A}}\, \hat{\mathbf{w}} = \bar{\mathbf{u}} \tag{23}$$

For a number $n_e = L$ of elements per stencil the matrix $\underline{\underline{A}}$ becomes square and easy invertible, but for realistic meshes this leads to an unstable scheme. So, to ensure the

robustness of the reconstruction we enlarge the stencils, see also [12]. The number of the elements per stencil is chosen as $n_e = 1.5L$ in 2D and $n_e = 2L$ in 3D. In addition the matrix can contain linear dependent rows due to geometrical reasons. This means that the reconstruction matrix $\underline{\underline{A}}$ may not be invertible. This is avoided by adding successively new elements to the stencil if one of the singular values of the matrix becomes zero. The overdetermined system (23) can be solved by an algorithm of singular value decomposition or, as it is done in our framework, by a least-squares method with the constraint (21).

The degrees of freedom $\hat{w}_{(i)}$ are now known, so the polynomials $w_{(i)}(\xi,\eta,\zeta)$ on each stencil are known and the final nonlinear reconstruction polynomial $w_{(i)}^{WENO}$ in the cell $C_{(i)}$ of degree M is defined by

$$w_{(i)}^{WENO}(\xi,\eta,\zeta) = \sum_{s=1}^{n_s} \omega_s w_{(i)_s}(\xi,\eta,\zeta) = \sum_{s=1}^{n_s}\sum_{l=1}^{L} \omega_s \hat{w}_{(i)_{s,l}} \Psi_l(\xi,\eta,\zeta). \tag{24}$$

Unlike the common ENO (Essentially Non Oscillatory) schemes, where only the less oscillating polynomial is chosen, all reconstruction polynomials on each stencil are taken into account by a linear combination as done in eq. (24) with the normalized nonlinear weights ω_s

$$\omega_s = \frac{\tilde{\omega}_s}{\sum\limits_{r=1}^{n_s} \tilde{\omega}_r} \qquad \text{with} \qquad \tilde{\omega}_s = \frac{\lambda_s}{(\varepsilon+\sigma_s)^r} \tag{25}$$

according to [11, 17, 4], whereas the non-normalized nonlinear weights $\tilde{\omega}_s$ depend on the linear weights λ_s and the oscillation indicators σ_s.

The parameters ε and r are set in the common range given in the literature [17, 4], i.e. $\varepsilon = 10^{-5} - 10^{-14}$ and $r = 2-8$. Thereby ε is regarded as a threshold for a division by zero which does not influence much the stability of the reconstruction scheme. The parameter r states the sensitivity of the nonlinear weights relative to the oscillation indicators σ_s. For bigger r the reconstruction procedure tends to an ENO behavior, whereas for smaller values the scheme becomes more oscillatory.

For the weights ω_s in (24) suitable oscillation indicators are necessary to ensure a robust reconstruction. In literature ([10, 12]) this is usually achieved by a scaling with the cell volume. As the reconstruction procedure is done in the reference coordinate system this is not necessary any more. Due to the definition of the polynomials (20) σ_s can furthermore be computed in a mesh independent way

$$\sigma_s = (\hat{\mathbf{w}}_s)^T \, \underline{\underline{\Sigma}} \, \hat{\mathbf{w}}_s \tag{26}$$

with $\hat{\mathbf{w}}_s$, the vector of the degrees of freedom of the polynom on the stencil m and $\underline{\underline{\Sigma}}$ the universal oscillation matrix defined by

$$\Sigma_{lk} = \sum_{r=1}^{M} \sum_{\alpha=0}^{r} \sum_{\beta=0}^{r-\alpha} \int_{C_U} \frac{\partial^r}{\partial \xi^\alpha \partial \eta^\beta \partial \zeta^\gamma} \Psi_l(\xi,\eta,\zeta) \cdot \frac{\partial^r}{\partial \xi^\alpha \partial \eta^\beta \partial \zeta^\gamma} \Psi_k(\xi,\eta,\zeta) d\xi d\eta d\zeta, \tag{27}$$

whereas $\gamma = r - \alpha - \beta$. As the reconstruction basis functions Ψ are generally given, the oscillation matrix is neither dependent on the mesh, nor on the problem, i.e. it can be computed and stored in advance of a computation, considerably increasing the efficiency of this reconstruction method.

In contrast to the common WENO schemes the linear weights are not used for the improvement of the accuracy as was shown by Liu, Osher and Chan [13] but simply defined by

$$\lambda_s = \begin{cases} \lambda_c & \text{if } s = 1, \text{ i.e. } c \text{ is the index of the central stencil,} \\ 1 & \text{else} \end{cases} \tag{28}$$

according to Dumbser et al. [4], with $\lambda_c \gg 1$, which puts a high emphasis on the central stencil. It was shown in [4] that a choice of $\lambda_c = 10^2 - 10^5$ does not show sensitivities in the results. Nevertheless, lower λ_c yield better results at discontinuities and larger weights are favorable for smooth solutions.

4 Numerical Results

For the validation of the implemented iterated defect correction method exhaustive studies have been made for 1D, 2D and 3D Euler and Navier-Stokes problems. All simulations have been carried out with a standard finite volume scheme using ghost cells to impose boundary conditions. Depending on the test case a first or a second order basic scheme was used, whereas for the defect correction a polynomial WENO reconstruction up to 6th order was applied with the standard choice for the reconstruction parameters shown in section 3. In this section we first show some of the convergence studies of those validation cases and we end up with application test cases.

4.1 Convergence Studies

To validate our proposed iterated defect correction method for inhomogeneous problems we took as a first example in 1D the nonlinear Euler equations where a source term $\mathbf{s}(\mathbf{u},A)$, depending on the solution $\mathbf{u}$ and a given geometry A, was added. The equations in (29) are derived from the homogeneous Euler equations in three dimensions with the assumption of a continuous area variation (see also [20]).

$$\mathbf{u}_t + \mathbf{F}(\mathbf{u})_x = \mathbf{s}(\mathbf{u}) \qquad \text{with} \qquad \mathbf{s} = -\frac{1}{A}\begin{pmatrix} \rho u A_x \\ \rho u^2 A_x \\ u(e+p)A_x \end{pmatrix} \tag{29}$$

This gives an approximation of a 2D axi-symmetric nozzle flow with the x-axis as nozzle symmetry and $A(x)$ as cross-sectional area along the nozzle. In our case we took a smooth sinus function

$$A(x) = \begin{cases} 2, & -1 \le x \le -\frac{1}{2} \\ 2 - sin^4\left(\pi(x+\frac{1}{2})\right), & -\frac{1}{2} < x < \frac{1}{2} \\ 2, & \frac{1}{2} \le x \le 1 \end{cases} \tag{30}$$

for the cross-sectional area which is illustrated in the upper left corner of Fig. 1. We took a subsonic expansion with inflow and outflow pressure $p = 1$ and an inflow velocity $u = 0.2$ with an inflow mass flow $\rho u = 0.28$. We obtain then an inflow Mach number of $Ma = 0.2$ which can be introduced into the 1D nozzle theory to evaluate the exact state at the inflow and outflow section. This is imposed during the simulations which result into a symmetrical distribution of the state variables (see Fig. 1). We can clearly see the difference between the first order basic method and the corrected solution in both amplitude and location of the peak which is expected to be in the nozzle throat at $x = 0$. In this case a cubic polynomial reconstruction was chosen to compute the local defect.

To measure the exact error between the approximated solution $\mathbf{u}_h$ and the exact solution $\mathbf{u}_e$ we use continuous L^p norms

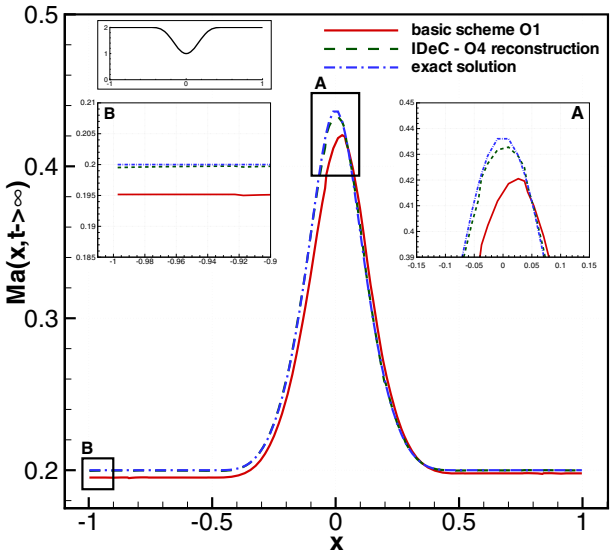

Fig. 1 Mach number distribution of a axi-symmetric nozzle flow simulated with a first order basic method and corrected by a fourth order polynomial reconstruction for the local defect

$$\| \mathbf{u}_h - \mathbf{u}_e \|_{L^p(\Omega)} = \left(\int_{\Omega} |\mathbf{u}_h - \mathbf{u}_e|^p dV \right)^{1/p}, \tag{31}$$

whereas the L^∞-norm gives the maximum absolute error arising in the whole domain. We compute the integral with the Gaussian quadrature algorithm with twice the number of Gauss points compared to the numerical scheme. For the defect correction it is important to make this analysis with the high order polynomials and, respectively, with the high order integration and not with the accuracy of the basic method. Table 1 shows the convergence tables of the nozzle test case for five successively refined grids. In addition to the fourth order defect reconstruction we show a convergence table for a first order basic method corrected with a 6th order reconstruction to determine the local defect.

The validation of the 2D and 3D implementation has been carried out by using the method of manufactured solutions, i.e. we insert an analytical function

$$\rho_e(x) = sin(\pi x) \cdot sin(\pi y) + 2$$

for the exact density distribution in 2D and respectively

$$\rho_e(x) = sin(\pi x) \cdot sin(\pi y) \cdot sin(\pi z) + 1$$

in 3D into the Euler equations and solve the inhomogeneous two-, respectively three-dimensional Euler equations

$$\mathbf{u}_t + \nabla \cdot \mathbf{F}(\mathbf{u}) = \mathbf{s}(\mathbf{x}). \tag{32}$$

Table 1 Iterated defect correction based on a first order steady solution with a 4th (up) and 6th (down) order reconstruction, 1D homogeneous grid, convergence rates of the mass flow variable

h	L^∞	L^1	L^2	$\mathscr{O}_{L^\infty}$	$\mathscr{O}_{L^1}$	$\mathscr{O}_{L^2}$
Basic method $\mathscr{O}1 \rightarrow$ IDeC with $\mathscr{O}4$ reconstruction						
0.080	7.69E-03	2.17E-03	2.64E-03	-	-	-
0.040	6.34E-04	1.26E-04	1.78E-04	3.6	4.1	3.9
0.020	3.46E-05	6.08E-05	9.69E-05	4.2	4.4	4.2
0.010	2.14E-06	3.19E-06	5.63E-06	4.0	4.3	4.1
0.005	1.35E-07	1.83E-07	3.44E-07	4.0	4.1	4.0
Basic method $\mathscr{O}1 \rightarrow$ IDeC with $\mathscr{O}6$ reconstruction						
0.100	8.80E-03	2.22E-03	2.49E-03	-	-	-
0.067	1.92E-03	2.95E-04	4.19E-04	3.8	5.0	4.4
0.033	6.66E-05	8.94E-06	1.54E-05	4.9	5.0	4.8
0.017	1.54E-06	1.80E-07	3.28E-07	5.4	5.6	5.6
0.008	2.63E-08	3.02E-09	5.58E-09	5.9	5.9	5.9

The remaining state variables like the velocity and the pressure were set to a constant value greater zero. For our choice we obtain source terms which in contrast to the one dimensional analysis depend only on the space

$$s_i = \pi \cdot sin(\pi x) \cdot cos(\pi y) + \pi \cdot cos(\pi x) \cdot sin(\pi y) \qquad \text{for} \qquad i = 1...4 \tag{33}$$

in two dimensions and respectively

$$\begin{aligned} s_i &= \pi \cdot sin(\pi x) \cdot sin(\pi y) \cdot cos(\pi z) + \pi \cdot sin(\pi x) \cdot cos(\pi y) \cdot sin(\pi z) \\ &+ \pi \cdot cos(\pi x) \cdot sin(\pi y) \cdot sin(\pi z) \qquad \text{for} \qquad i = 1...4 \\ s_5 &= \frac{3\pi}{2} \cdot sin(\pi x) \cdot sin(\pi y) \cdot cos(\pi z) + \frac{3\pi}{2} \cdot sin(\pi x) \cdot cos(\pi y) \cdot sin(\pi z) \\ &+ \frac{3\pi}{2} \cdot cos(\pi x) \cdot sin(\pi y) \cdot sin(\pi z) \end{aligned} \tag{34}$$

in three dimensions. For the simulations we initialized the domain $\Omega_{2D} = [0;1]x[0;1]$ in 2D and respectively $\Omega_{3D} = [0;1]^3$ in 3D with the exact solution and iterated the basic scheme to a steady state with the exact solution imposed on the boundaries. The same convergence study as in one dimension based on the L^p-norms was carried out on four successively adapted grids. In all our computations we used fully unstructured grids with irregular triangles in two dimensions and tetrahedrons in three dimensions. Each adaptation is performed globally, i.e. we applied the so-called red-refinement in each cell of the domain per adaptation step. An example of two adaptation steps is shown for the three dimensional case in Fig. 2.

Again we can see the difference between the solution of the basic method and the corrected one. This is demonstrated for the two dimensional case for the density distribution in Fig. 3. We have to mention that for the visualization of the higher order solutions we subdivide the numerical grid and write out the value of the polynomial distribution at each barycenter center of the subdivided grid. In this way we can see the Godunov approach of constant values in the cell for the first order solution (Fig. 3, left) and the continuous fourth order solution with vanishing jumps between the cells (Fig. 3, right). A quantitative analysis can be done by determining the convergence rates for the corrected solutions as it was done in the one dimensional case. In Tab. 2 we show the experimental convergence order for the two- and

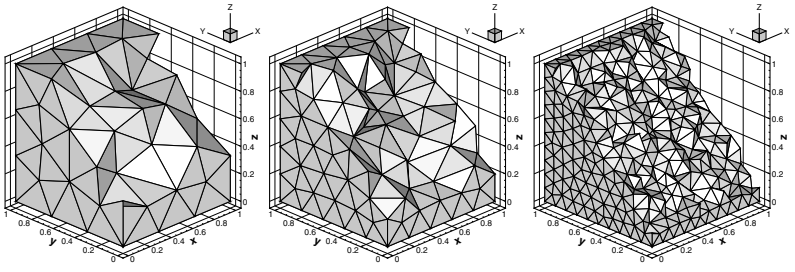

Fig. 2 Grid topologies used for the convergence studies in three dimensions

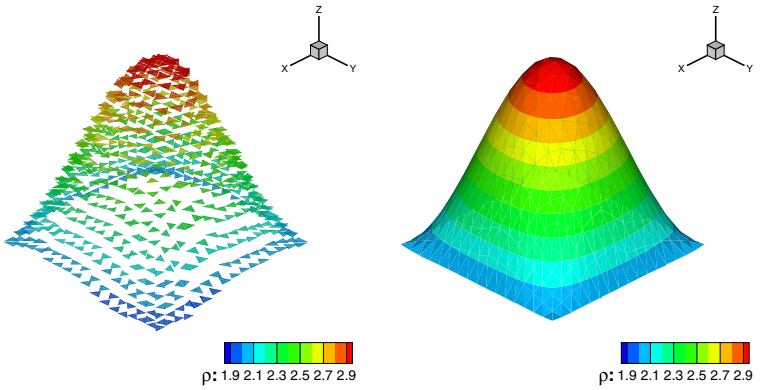

Fig. 3 Solution of the first order basic scheme (left) and the corrected solution of an IDeC with a 4th order polynomial reconstruction for the local defect (right)

three dimensional simulations where we used a first order basic scheme with a cubic polynomial reconstruction for the defect correction. In both cases we reach the optimal theoretical convergence order of $M+1$ when iterated defect correctionis applied. The convergence rates can approve that with the mesh step size $h \to 0$ the error tends towards zero with the potential power of $M+1$, M being the polynomial degree of the reconstruction basis polynomials Ψ (see chapter 3). However, nothing can be said about the real simulation time needed by the employed numerical scheme and with it the real gain of using a higher order reconstruction. Therefore we show in Fig. 4 the L^1-norm of the errors for the one and two dimensional computations described above over the total CPU-time in seconds needed

Table 2 Density convergence rates for IDeC with a first order basic scheme and a cubic polynomial reconstruction on 2D (up) and 3D (down) irregular unstructured grids)

h	L^∞	L^1	L^2	$\mathscr{O}_{L^\infty}$	$\mathscr{O}_{L^1}$	$\mathscr{O}_{L^2}$
2D Basic scheme $\mathscr{O}1 \to$ IDeC with $\mathscr{O}4$ reconstruction						
0.191	7.55E-02	1.06E-02	1.45E-02	-	-	-
0.096	5.78E-03	4.68E-04	7.12E-04	3.7	4.5	4.4
0.048	7.07E-04	2.95E-05	4.91E-05	3.0	4.0	3.9
0.024	4.97E-05	1.69E-06	3.17E-06	3.8	4.1	3.9
3D Basic scheme $\mathscr{O}1 \to$ IDeC with $\mathscr{O}4$ reconstruction						
0.182	5.67E-02	9.49E-03	1.22E-02	-	-	-
0.127	9.69E-03	1.87E-03	2.39E-03	5.0	4.6	4.6
0.068	8.71E-04	1.01E-04	1.32E-04	3.8	4.6	4.6
0.035	8.38E-05	7.09E-06	9.54E-06	3.6	4.1	4.0

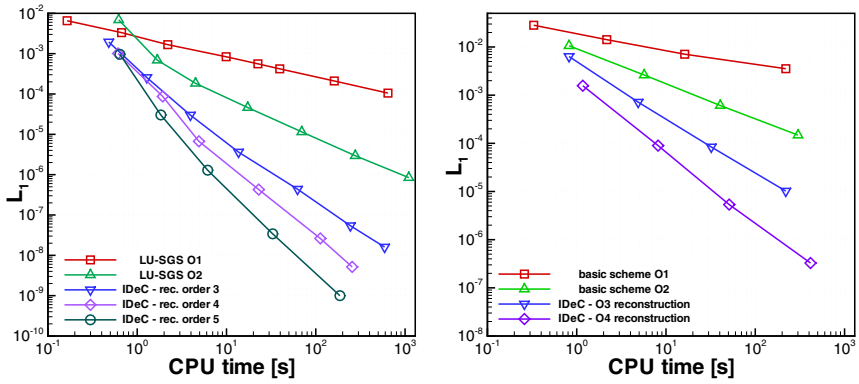

Fig. 4 Convergence rates over total CPU time for first and second order methods compared to iterated defect correction with higher order reconstruction in 1D (left) and 2D (right)

for a converged iterated defect correction and the basic schemes of first and second order. The simulations were all performed on one single AMD Athlon 5200+ processor with 3GB of RAM. So we can compare directly the computational effort to reach the same given accuracy of the L^1-norm. To give an example, if we want to reach an error norm of $L^1 = 10^{-4}$ in the one dimensional case (Fig.4, left), we obtain a speed up of factor 4 comparing a second order scheme with a third order corrected solution based on a first order basic scheme. The same comparison for the two dimensional case leads even to a speed up of factor 20 which is due to higher computational cost for the 2D simulations concerning for example the integration (Fig.4, right). This results for the speed up are surely dependent on the test case, nevertheless they give an idea of the potential of higher order schemes. However, in the one dimensional test case we can see, that the speed up of a higher order scheme starts to be significant for very low accuracy levels.

A more demanding test case for the stability and the convergence of the iterated defect correction for the steady nonlinear Euler equations is the Ringleb's flow [2]. It is one of the few continuous transonic flows of a blunt obstacle which can be solved analytically with the Hodograph method in a transformed $(V - \theta)$ plane, with V as the velocity magnitude and θ the angle of the velocity with respect to x-axis. More details on the Hodograph method and the analytical solution can be found in [2]. In our case the flow direction is upwards with the wall boundaries left and right. Their topology is derived from the analytical solution where the chosen boundaries of our test case represent two stream lines. The inflow and outflow boundaries are circles also given by the exact solution. The chosen geometry leans on th article [21].

In spite of being a transonic flow, it is smooth in the whole domain and since we can compute an exact solution at each grid point there is also a quantitative analysis possible. In addition the flow is supposed to be irrotational and isentropic. We performed the simulations on three successively adapted regular triangular grids imposing the exact solution on every boundary. Starting from the exact solution as

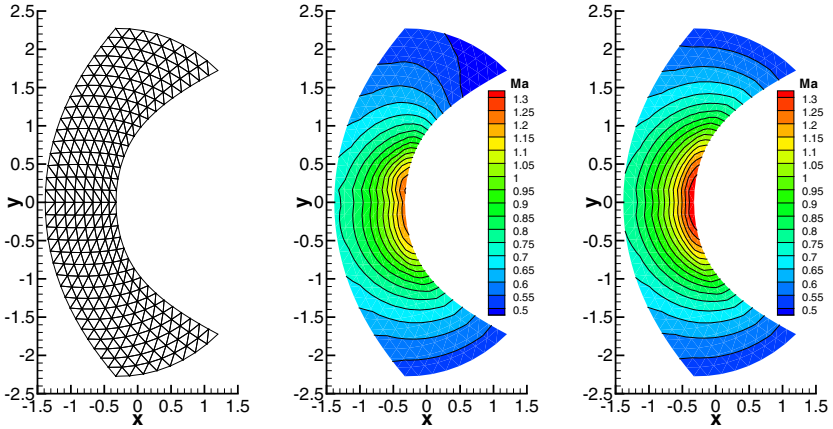

Fig. 5 One of the used triangular grids, steady solution of the first order basic method (middle) and defect correction solution with 4th order reconstruction (right)

the initial condition we use a first order scheme as the basic method for the iteration to a steady solution. In Fig. 5 the middle fine grid is depicted together with the steady solution of the basic method and the solution corrected with IDeC. We expect a complete symmetrical solution with a defined circular sonic line. The first order basic method clearly failures in these flow topologies. There are small instabilities, nevertheless the method is stable and converges perfectly, which is important for the method of iterated defect correction. For the defect correction we applied a 4th order accurate WENO reconstruction with the parameters $n_e = 2L$, $r = 6$, $\varepsilon = 10^{-14}$ and $\lambda_c = 10^5$.

With the IDeC we get a good solution which is near to the exact one in spite of the unsymmetrical solution of the basic method. With this setup we reach the theoretical convergence order of the reconstruction, proving the possibilities of the iterated defect correction method. If we compare the absolute error L^p-norms (Tab. 3) of both solutions this means a correction of the basic scheme from one up to four orders of magnitude for the finest grid.

Beside the nonlinear Euler equations we applied the method of iterated defect correction on the Navier-Stokes equations as well. Similar to the convergence studies shown before, we used the method of manufactured solution and solved

$$\mathbf{u}_t + \nabla \cdot \mathbf{F}(\mathbf{u}, \nabla \mathbf{u}) = \mathbf{s}(\mathbf{x}) \tag{35}$$

with $\mathbf{F}(\mathbf{u}, \nabla \mathbf{u}) = \mathbf{F}^c(\mathbf{u}) - \mathbf{F}^d(\mathbf{u}, \nabla \mathbf{u})$, where $\mathbf{F}^c$ and $\mathbf{F}^d$ denote the convective respectively the diffusive flux. The defect correction formulation in (11) does not change in the case of solving the Navier-Stokes equation, but is just extended by the diffusive flux what results in

Table 3 Convergence rates for the first order basic method (up) and the corrected solution with 4th order reconstruction (down)

N	L^∞	L^1	L^2	$\mathscr{O}_{L^\infty}$	$\mathscr{O}_{L^1}$	$\mathscr{O}_{L^2}$
Basic method $\mathscr{O}1$						
32	5.55E-02	5.89E-02	3.68E-02	-	-	-
64	3.56E-02	3.14E-02	2.01E-02	0.9	0.9	0.6
128	2.20E-02	1.64E-02	1.06E-02	0.9	0.9	0.7
Basic method $\mathscr{O}1 \rightarrow$ IDeC with $\mathscr{O}4$ reconstruction						
32	4.17E-03	9.55E-04	8.10E-04	-	-	-
64	3.23E-04	4.10E-05	4.04E-05	3.7	4.5	4.3
128	1.90E-05	2.07E-06	2.04E-06	4.1	4.3	4.3

$$R(\mathscr{Q}_i) = \int_{t^n}^{t^n+\Delta t} \int_{x_{i-1/2}}^{x_{i+1/2}} f^c(\mathscr{Q}_i)_x dx dt + \int_{t^n}^{t^n+\Delta t} \int_{x_{i-1/2}}^{x_{i+1/2}} f^d(\mathscr{Q}_i, (\mathscr{Q}_i)_x)_x dx dt \tag{36}$$

with $\mathscr{Q}_i$ still acting as a placeholder for $u_i^{[k]}, u_i^{[k+1]}$ and $w_i^{[k]}$. Similar to the Euler equations the local defect is now computed for both fluxes, the convective and the diffusive flux. A high order formulation for the diffusive flux is therefore necessary. We have chosen the approximation suggested by Gassner et al. in [8]. It enables a one-step numerical method of high order accuracy in space and time using the same data as for the convection flux. Based on the idea of Godunov for advection problems not with constant initial data but with a linear initial distribution, it results in the so-called diffusive generalized Riemann problem (dGRP). Solving this Riemann problem yields two parts, the one containing the arithmetic mean value of the first derivative, whereas the second contains a physically motivated limiting term composed of the jump in the state of two adjacent cells. In 2D and 3D this leads to

$$\int_{\partial C_i} g\left(w_i^{[k]}, \nabla w_i^{[k]}\right) \mathbf{n} dS \approx \sum_{K \in \partial C_i} \sum_{j=1}^{n_{GP}} \omega_j^K g_{\mathbf{n}^K}\left(w_{i,j}^{[k]}, \left(w_{i,j}^{[k]}\right)_{n^K}\right) S_K \tag{37}$$

with

$$\left(w_{i,j}^{[k]}\right)_{n^K} = \frac{1}{2}\left(\frac{\partial}{\partial n} w_{i,j}^{[k],+} + \frac{\partial}{\partial n} w_{i,j}^{[k],-}\right) + \eta\left(w_{i,j}^{[k],+} - w_{i,j}^{[k],-}\right) \tag{38}$$

a numerical approximation for the diffusion flux, $\partial/\partial n$ denoting the derivative in normal direction. The characteristic length h is taken as twice the distance from the barycenter of the cell C_i to the barycenter of the edge K of the computed flux. The integration is again done by Gaussian quadrature with ω_j^K the weights on the edge K using a total number n_{GP} of integration points. The jump in the state of two neighboring cells is multiplied by the parameter η

$$\eta = \frac{1}{h\sqrt{\frac{1}{2}\pi}} \tag{39}$$

which can also be interpreted as a penalty term for the jump. With the chosen WENO reconstruction we obtain the derivative directly from the reconstructed polynomial distribution. However, the theoretical convergence order for this flux is limited to M, the degree of the reconstruction polynomials, in the case of a finite volume method. This is due to the fact that we use the first derivation of our polynomials losing hence one order of accuracy (see also [8]).

As an exact solution for the iterated defect correction applied on the Navier-Stokes equations simulated in two dimensions we took

$$\mathbf{u}_e = \begin{pmatrix} sin(\pi x)sin(\pi y)+4 \\ sin(\pi x)sin(\pi y)+4 \\ sin(\pi x)sin(\pi y)+4 \\ (sin(\pi x)sin(\pi y)+4)^2 \end{pmatrix} \tag{40}$$

with $\mathbf{u} = (\rho, \rho u, \rho v, \rho e)^T$ denoting the vector of the conservative state. By inserting (40) into (35) we can again compute the source term $\mathbf{s}$, which is only a function of the space $\mathbf{x}$. To test the method of iterated defect correction for rather viscous flows we chose a viscosity $\mu = 10^{-1}$, which results in a very low Reynolds number of $Re = 80$. As the temperatures are very low and do not take effect on the viscosity, we performed these computations with the assumption of a constant μ. The simulations were all carried out on a fully periodic domain $\Omega = [0;2]x[0;2]$ with periodic boundaries on successively adapted regular triangular grids.

As we use the derivative of the polynomial distribution for the flux approximation we have to take a basis scheme with at least second order of accuracy for the defect correction. In Tab. 4 we show the convergence rates of the test case above computed with a second order basis method and corrected by a local defect using a 4th order reconstruction. Motivated by several assumptions found in the literature on the numerical error which is supposed to be dominated by the convection part we could think of dividing the local defect into an convective and a diffusive part. As both can be computed independent from another we performed the same simulation

Table 4 Convergence rates computed for the pressure for a second order basic method and a defect correction with 4th order reconstruction

h	L^∞	L^1	L^2	$\mathscr{O}_{L^\infty}$	$\mathscr{O}_{L^1}$	$\mathscr{O}_{L^2}$
Basic method $\mathscr{O}2 \rightarrow$ IDeC with $\mathscr{O}4$ reconstruction						
0.200	2.05E-01	1.95E-01	1.23E-01	-	-	-
0.100	1.40E-02	1.36E-02	8.63E-03	3.9	3.8	3.8
0.050	8.87E-04	8.84E-04	5.54E-04	4.0	3.9	4.0
0.025	5.81E-05	5.49E-05	3.46E-05	3.9	4.0	4.0

Table 5 Convergence rates for the second order basic method (up) and the corrected solution with 4th order reconstruction (down) and a local defect computed only from the convection flux

h	L^∞	L^1	L^2	$\mathscr{O}_{L^\infty}$	$\mathscr{O}_{L^1}$	$\mathscr{O}_{L^2}$
Basic method $\mathscr{O}2$						
0.200	6.69E-01	6.27E-01	3.99E-01	-	-	-
0.100	1.78E-01	9.66E-02	1.51E-01	1.9	2.0	2.0
0.050	4.66E-02	3.85E-02	2.44E-02	1.9	2.0	2.0
0.250	1.42E-02	1.04E-02	6.50E-03	1.9	1.9	1.9
Basic method $\mathscr{O}2 \rightarrow$ IDeC with $\mathscr{O}4$ reconstruction						
0.200	2.01E-01	1.94E-01	1.22E-01	-	-	-
0.100	2.15E-02	2.33E-02	1.41E-02	3.2	3.1	3.1
0.050	7.08E-03	8.00E-03	4.77E-03	1.6	1.5	1.6
0.250	2.91E-03	3.70E-03	2.18E-03	1.3	1.1	1.1

as before, with a local defect defined only in the convection flux setting the local defect of the diffusion to zero.

From the convergence rates in Tab. 5 one can see that for low Reynolds numbers, i.e. for flows dominated by the viscosity, it is indispensable to compute the local defect also for the diffusive fluxes to reach the optimal order of convergence. However, the absolute error norms of the corrected solution are lower than the ones of the basic method computed with second order accuracy. That means, by taking into account only the local defect of the convective flux we can not reach the full optimal convergence order but we obtain a slightly better solution than that computed with the basic method.

4.2 Application Test Cases

4.2.1 The RAE 2822 Profile

As a first application test case for the method of iterated defect correction we simulated the flow around the RAE 2822 profile in two dimensions. It is one of the official test cases of the project MUNA. We solve only the nonlinear Euler equations for this test case, so the grid we used is fully unstructured and contains about 18.000 elements with a relatively high discretized profile of 180 points per each half of the profile. The farfield is situated at 40 cord lengths and the profile is simulated as slip wall with the velocity normal to the wall set to zero. The flow was defined by the flow conditions of the so-called test case 9 with $Ma = 0.73$ and an incident angle $\alpha = 2.78^\circ$. This yields a transonic flow with a shock on the upper side of the profile (see Fig. 6, right). To compare the solution of the iterated defect correction we performed the simulation on the same grid with the numerical code of the DLR

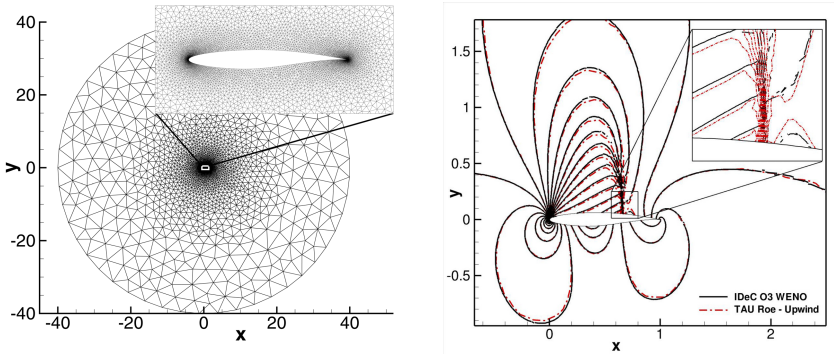

Fig. 6 Fully unstructured grid for the RAE 2822 profile (left) and Mach number distribution of the corrected solution and a direct solution with the TAU code using a second order TVD upwind scheme (right)

("Deutsches Zentrum für Luft- und Raumfahrt"), the TAU code, used as standard code for the project MUNA. The parameters for the TAU code were set to a second order TVD scheme with a least squares reconstruction and the Roe approximation for the convective flux.

In the case of iterated defect correction we used a first order basic method and corrected the steady solution by a local defect reconstructed with the WENO method described in section 3 using polynomials of degree two. The difference between the basic method and the corrected solution can be seen for the aerodynamic coefficients. In Fig. 7 we show the lift and drag coefficients over the number of iterations. Our iterative method is a rather suboptimal explicit method and so the number of iterations needed for a steady solution is quite high but does not influence the defect correction and is not of interest here. When the solution does not change any more we compute the local defect and solve afterwards the modified equations (5) to obtain a corrected solution which is denoted by the small arrows in Fig. 7. So each small arrow stands for a defect correction iteration.

We can see that the lift coefficient could already be corrected to the end solution after just one defect correction, whereas the drag coefficient needs some more defect correction iterations to converge. In the case of the lift coefficient a correction of about 11% was obtained and the drag coefficient could be corrected with even 28% of the first order solution, what corresponds to a total reduction of around 80 drag counts. The results of the TAU code serve here not only for validation but as a comparison as well, not having an exact solution for this test case.

In addition to the aerodynamic coefficients we can clearly see that by the iterated defect correction method with a 3rd order WENO reconstruction the shock is better resolved than it is with the second order least squares in the TAU code (see Fig. 6, right). Only if we once adapt the grid globally we are able to reach approximately the same shock resolution with the second order scheme.

4.2.2 Laminar Boundary Layer at High Reynolds Number

For the second application we solve the compressible Navier-Stokes equations at a low Mach number for a classical test case, the flow over a flat plate. We are simulating a laminar boundary layer but for a very high high Reynold number. Ludwig Prandtl and Blasius, one of his students, made pioneering achievements with their work on the boundary layer. This ended up in the solution of Prandtl's boundary layer approximation equations by Blasius, reducing them to a nonlinear ordinary differential equation (ODE) of third order for the case of a laminar steady flow. This ODE can be solved nowadays numerically by a math algebra program with an arbitrary accuracy. We employed the software Matlab where we solved Blasius' boundary layer equations (see e.g. [16]) with a four step Runge-Kutta scheme and a Newton-Raphson iteration method. This serves us as the reference solution for the iterated defect correction applied on the Navier-Stokes equations.

To point out the abilities of the WENO reconstruction in a reference space used in our work and the approach of the iterated defect correction we still used a fully unstructured triangular grid even in the boundary layer. For a finite volume scheme, this is a quite demanding task where surely some extra fine tuning is necessary to obtain satisfying results. One of them turned out to be the numerical flux approximation for which we took the HLLC flux as described in [20]. Our computational domain is $\Omega = [-0.5, 2]\mathrm{x}[0, 0.05]$ discretized by a total of 5250 triangular elements. In the interval $-0.5 < x < 0$ we use a slip wall boundary condition where the velocity normal to the wall is zero. At $x = 0$ we impose than a non-slip wall adiabatic boundary condition in the interval $0 < x < 2$. The free stream Mach number is $Ma_\infty = 0.3$, resulting from the free stream flow parallel to the wall with $u_\infty = 0.3$, $\rho_\infty = 1$ and $p_\infty = 1/\gamma$. As we use the equation of state for ideal gas the ratio of the specific heats is $\gamma = 1.4$, whereas the Prandtl number is $Pr = 1$.

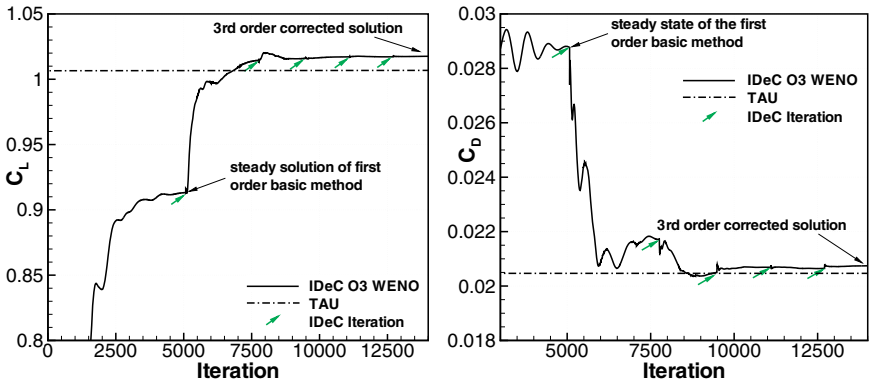

Fig. 7 Lift (left) and drag (right) coefficient computed with a first order basic method and a 3rd order defect reconstruction, compared with a second order TAU code solution on the same grid

For the chosen high Reynolds number of $Re = 10^6[1/m]$ we set our viscosity to $\mu = 3 \cdot 10^{-7}$ making again the assumption of a constant viscosity in the whole domain. To resolve the flow at high Reynolds numbers, which implies a very thin boundary layer of $\delta_{x=1} = 5 \cdot 10^{-3}$ in our case, a highly stretched grid in the boundary layer is necessary. At $x = 1$ we therefore have cells with an aspect ratio of $1 : 205$. However the chosen spacing at the first cell of $y_1 = 4 \cdot 10^{-4}$ is still quite high compared to setups in the literature which are meant to be solved with a finite volume method 2nd order TVD method (see e.g. [9]). In addition we use only 8-9 cells to discretize the boundary layer at $x = 1$.

The initial condition is given by the free steam conditions and we take a homogeneous block profile with the free stream conditions at the inflow. It is important that mass can escape at the farfield, since due to the boundary layer growth we get a non-zero velocity outwards. At the outflow we can use simple extrapolation of the inner state values and impose only the free stream pressure. For the computation we used a second order basic scheme to obtain a steady solution which we reach after $t = 20$ seconds of simulation time. After each steady solution we apply the defect correction with a 4th order accurate WENO reconstruction again with the parameters $n_e = 2L$, $r = 6$, $\varepsilon = 10^{-14}$ and $\lambda_c = 10^5$. Left in Fig. 8 we see the distribution of the dimensionless x-velocity u/u_∞ in the whole domain for the basic method. In addition we compare the Blasius solution with the velocity profiles of both u and v components of the velocity at the position $x = 0.7$ (see Fig. 9) and with the skin friction coefficient over the entire plate (see Fig. 8, right). For all comparisons the corrected numerical solution, here shown after four defect correction iterations, is in good agreement with the Blasius reference solution. At this point, we have to mention, that using a scheme of higher order with WENO reconstruction is unstable and

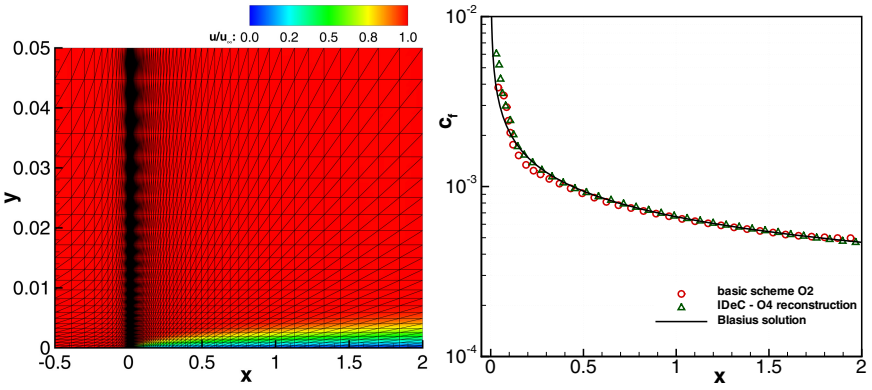

Fig. 8 Flat plate at high Reynolds number $Re = 10^6[1/m]$ with $\alpha = 0^\circ$ and $Ma = 0.3$ computed with a 2nd order basic method and corrected using a 4th order WENO reconstruction. Left we show the distribution of the dimensionless x-velocity u/u_∞ in the whole computational domain and right the skin friction coefficient is depicted over the plate length after four defect correction iterations.

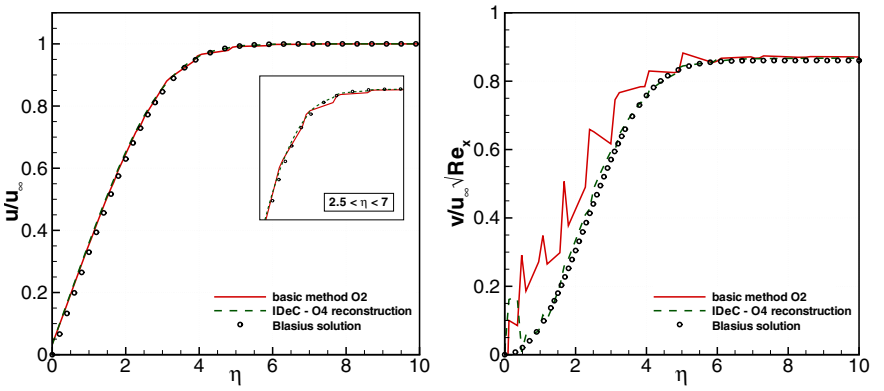

Fig. 9 Flat plate at high Reynolds number $Re = 10^6[1/m]$ with $\alpha = 0^\circ$ and $Ma = 0.3$ computed with a 2nd order basic method and corrected using a 4th order WENO reconstruction. Distribution of the dimensionless x-velocity u/u_∞ (left) and of the dimensionless y-velocity $v/u_\infty\sqrt{Re_x}$ (right).

no steady solution can be obtained. The method of iterated defect correction seems to be stable, as it is based only on a second order scheme, and is nevertheless able to correct the basic method with the high order accurate defect.

For the u component we can see in the zoom made in the section of the dimensionless variable $2.5 < \eta < 7$ with $\eta = y/\sqrt{\frac{\nu x}{u_\infty}}$ and the kinematic viscosity $\nu = \mu/\rho$, that we get a smoother distribution by applying the defect correction. In the case of the dimensionless v component of the velocity $v/u_\infty\sqrt{Re_x}$ with $Re_x = \sqrt{\frac{u_\infty x}{\nu}}$ the improvement of the solution is considerable. The completely wrong distribution of the basic method could be corrected to fit quite well with the reference Blasius solution. Near the wall we nevertheless reach the limits of the reconstruction, which has shown so far that the reconstruction in the reference space can cope even with these highly stretched elements. The corrected skin friction coefficient (Fig. 8, right) shows also better agreement with the reference solution especially at the beginning and the end of the plate. The remaining difference is due to the stagnation point at $x = 0$ where high gradients occur, causing oscillations. As can be read in literature the prediction of skin friction coefficients still remain a difficult issue in the numerical simulation. Similar to [9] we compare therefore the friction coefficients at the end of the plate at $x = 2$. The analytical solution can again be computed by solving the Blasius equations and we get

$$c_f = \frac{0.664}{\sqrt{Re_x}} \qquad \text{with} \qquad Re_x = \frac{\rho u_\infty x}{\mu}. \tag{41}$$

With $c_f(x = 2) = 4.983 \cdot 10^{-3}$ the error of the skin friction of the basic method is of 6.1% and with the iterated defect correction approach it could be corrected to $c_f(x = 2) = 4.653 \cdot 10^{-3}$ resulting in a remaining error of 0.9% for this case.

4.3 Conclusion

In this work we applied the method of iterated defect correction to a finite volume scheme and solved both, the Euler and the Navier-Stokes equations. A steady solution of lower accuracy, mostly of first or second order, is the starting point for the method of iterated defect correction. The next step consists of a WENO reconstruction which is used to evaluate the local defect of the steady solution. If we modify our equations by putting the local defect on the right hand side as a negative source term, the low order solution can be iteratively shifted to the accuracy of the reconstruction. The main advantage of this approach is that the high order scheme has not to be solved - the high order scheme is only used to calculate an estimation of the local discretization error. Hence, this approach can be used to increase the accuracy of an existing code in a straightforward way. It seems that the high order approximation also inherits some additional stability from the low order solver. Our results show that the iterated defect correctionin combination with the WENO reconstruction in [4] for unstructured meshes works very well. We did not succeed to define robust boundary conditions in any case. This seems to be even more subtle than the definition of high order boundary conditions in general.

We have shown numerical convergence results up to sixth order of accuracy, applying the method of iterated defect correction starting with a first order steady solution. By modifying the original approach, a relevant speed up could additionally be achieved for equations with source terms depending on the solution itself. The scheme remained stable even for the more challenging test case of the transient Ringleb's flow. A fourth order accurate solution could be achieved here from a first order numerical scheme. Convergence studies using the manufactured solutions method have shown that in the case of the Navier-Stokes equations, where a local defect can be computed separately for the convective and the diffusive fluxes, it is crucial for flows with low Reynolds numbers to evaluate the local defect for all fluxes. Neglecting the defect in the convective fluxes still gave better absolute error norms compared to the low order solution, but the expected high order of the reconstruction was not reached for our test cases.

A RAE 2822 profile have been computed as an application test case, solving the Euler equations with a first order basic scheme applying a third order accurate reconstruction to determine the local defect. Compared to the first order solution the aerodynamic coefficients like lift and drag could be corrected by 11%, respectively 28%. As a second application test case a laminar boundary layer at a high Reynolds number of $Re = 10^6$ was numerically solved using the iterated defect correction. Better results compared with the second order starting solution could be achieved applying the defect correction combined with a fourth order reconstruction. For example a reduction of the skin friction error at the end of the plate from 6.1% with the basic scheme to 0.9% was reached in this case.

References

[1] Abgrall, R.: On essentially non-oscillatory schemes on unstructured meshes: analysis and implementation. Journal of Computational Physics 144, 45–58 (1994)

[2] Chiocchia, G.: Exact solutions to transonic and supersonic flows. AGARD Advisory Report AR-211, pp. 1–14 (1985)

[3] Cockburn, B., Karniadakis, G., Shu, C.: Discontinuous Galerkin Methods. Lecture Notes in Computational Science and Engineering. Springer (2000)

[4] Dumbser, M., Käser, M.: Arbritrary high order non-oscillatory finite volume schemes on unstructered meshes for linear hyperbolic systems. Journal of Computational Physics 221(2), 693–723 (2007)

[5] Frank, R.: The method of iterated defect-correction and its application to two-point boundary value problems (part 1). Numer. Math. 25, 409–419 (1976)

[6] Frank, R.: The method of iterated defect-correction and its application to two-point boundary value problems (part 2). Numer. Math. 27, 407–420 (1977)

[7] Frank, R., Ueberhuber, C.W.: Iterated defect correction for differential equations part i: theoretical results. Computing 20, 207–228 (1978)

[8] Gassner, G., Lörcher, F., Munz, C.D.: A contribution to the construction of diffusion fluxes for finite volume and discontinuous galerkin schemes. Journal of Computational Physics 224, 1049–1063 (2007)

[9] Hirsch, C.: Numerical Computation of Internal and External Flows, vol. 1. Wiley (1989)

[10] Hu, C., Shu, C.: Weighted essentially non-oscillatory schemes on triangular meshes. Journal of Computational Physics 150, 97–127 (1999)

[11] Jiang, G., Shu, C.: Efficient implementation of weighted ENO schemes. Journal of Computational Physics, 202–228 (1996)

[12] Käser, M., Iske, A.: ADER schemes on adaptive triangular meshes for scalar conservation laws. Journal of Computational Physics 205, 486–508 (2005)

[13] Liu, X., Osher, S., Chan, T.: Weighted essentially non-oscillatory schemes. Journal of Computational Physics 115, 200–212 (1994)

[14] Pereyra, V.: Iterated deferred corrections for nonlinear boundary value problems. Numer. Math. 11, 111–125 (1968)

[15] Pereyra, V.L.: On improving an approximate solution of a functional equation by deferred corrections. Numer. Math. 8, 376–391 (1966)

[16] Schlichting, H.: Boundary Layer Theory, 7th edn. Springer (1979)

[17] Shu, C.: Essentially non-oscillatory and weighted essentially non-oscillatory schemes for hyperbolic conservation laws. NASA/CR-97-206253 ICASE Report No.97-65 (1997)

[18] Stetter, H.: Economical global error estimation. In: Willoughby, R.A. (ed.) Proceedings of the International Symposium on Stiff Differential Systems. Plenum Press, New York (1974); Wildbad, Germany (1973)

[19] Stetter, H.J.: The defect correction principle and discretization methods. Numer. Math. 29, 425–443 (1978)

[20] Toro, E.: Riemann solvers and numerical methods for fluid dynamics. Springer, Heidelberg (1997)

[21] Wang, Z., Liu, Y.: Extension of the spectral volume method to high-order boundary representation. Journal of Computational Physics 211, 154–178 (2006)

[22] Zadunaisky, P.: A method for the estimation of errors propagated in the numerical solution of a system of ordinary differential equations. In: Proceedings of the International Astronomical Union, Symposium, vol. 25. Academic Press, New York (1966)
[23] Zadunaisky, P.E.: On the estimation of errors propagated in the numerical integration of ordinary differential equations. Numer. Math. 27, 21–39 (1976)